Nano Energy 36 (2017) 110–117

Contents lists available at ScienceDirect

Nano Energy

journal homepage: www.elsevier.com/locate/nanoen

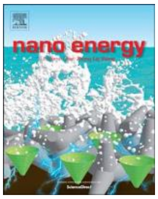

Full paper

Cyclic alkyl chains promote the polymer self-assembly and packing orders for solar cells

Liangliang Han[a], Huanxiang Jiang[a], Dan Ouyang[a], Weichao Chen[a,d], Tong Hu[b], Junyi Wang[a], Shuguang Wen[a], Mingliang Sun[b], Renqiang Yang[a,c,*]

[a] *CAS Key Laboratory of Bio-based Materials, Qingdao Institute of Bioenergy and Bioprocess Technology, Chinese Academy of Sciences, Qingdao 266101, China*
[b] *Institute of Material Science and Engineering, Ocean University of China, Qingdao 266100, China*
[c] *State Key Laboratory of Luminescent Materials and Devices, South China University of Technology, Guangzhou 510641, China*
[d] *College of Textile & Clothing, Qingdao University, Qingdao 266071, China*

ARTICLE INFO

Keywords:
Cyclic alkyl chains
Self-assembly
Polymer solar cells
Organic photovoltaics
Phase separation

ABSTRACT

The micro-structure ordering of the π−conjugated polymer film self-assembling from solution governs its electrical characteristics and performances for organic electronics. The side chains appended on the conjugated backbone could impact the self-assembling characteristics of the polymer, which show us how to design novel substituents to optimize the polymer arrangement and packing in its solid state. Here, cyclic alkyl chains are proven to be excellent ones for designing of narrow bandgap polymers, the design feature of which with preferential conformations can promote the polymer self-assembly and result in higher degree of lamellar order as well as tighter lamellar packing in the active layer, comparing with linear alkyl chains. The linear ones have poorer ordering in the polymer:fullerene blends as well as in the single crystals of the monomers. The well-organized polymer micro-structures facilitate polymer:fullerene phase separation together with balanced hole/electron transporting, and ultimately, improve the power conversion efficiency impressively compared to linear chains.

1. Introduction

Bulk heterojunction (BHJ) polymer solar cells (PSCs) have already aroused great concern in the recent twenty years, because of their bright future in realization of a printable, flexible and renewable energy source [1–3]. The π−conjugated polymer and fullerene derivative mixed into a specific solvent, and then spin coated to fabricate a film with thickness of 100 nm to 1 µm, which could absorb sunlight, create and transport charge carriers, finally, form an external circuit [4]. Any of these physical processes will significantly influence the open-circuit voltage (V_{OC}), the short-circuit current density (J_{SC}) and the fill factor (FF) of a PSC device. The π−conjugated polymer self-assembling as the solvent evaporating determines the film-forming property, micro-structure and phase separation in the polymer:fullerene blends, which governs the performances of the solution processed PSCs [5–9]. By optimizing the motifs of the π−conjugated backbones and patterns of the alkyl side chains, as well as hand-picking the film processing conditions that could direct the polymer arrangement and stacking, the power conversion efficiencies (PCEs) of the state-of-the-art PSCs have exceeded 10% and always been ongoing [10–13].

Over the years, a number of studies have emphasized that the alkyl side chains could impact the organization of the π−conjugated polymers, and in turn, influence their electrical conductivity [14], carrier mobility [15,16] and PCE [17–20]. The uniform alkyl side chain arrangement could promote side chain inter-chain interdigitation, degree of lamellar order and packing of backbones, ultimately, facilitate high performances of the polymer based organic electronics [21–23]. However, these insulated and unconjugated *n*- or *iso*-alkyl chains are flexible and always adopt variable twisted conformations beyond their ideal linear “zigzag” conformation appending on the organic semiconductors [24–27], showing high degree of disorder, which, in actuality, may destroy the pristine π−conjugated skeleton arrangement and decrease their ordered self-assembly. Thus, improving the order of alkyl chains may be interesting, and possibly, could weaken the resistance and lead to higher degree of ordered self-assembly. Cyclic alkyl chains are the analogs of *n*- and *iso*-alkyl chains, but, they adopt preferential conformations, exhibiting better symmetry and stronger rigidity. However, π−conjugated polymers appended with these cyclic

---

[*] Corresponding author at: CAS Key Laboratory of Bio-based Materials, Qingdao Institute of Bioenergy and Bioprocess Technology, Chinese Academy of Sciences, Qingdao 266101, China.

E-mail address: yangrq@qibebt.ac.cn (R. Yang).

http://dx.doi.org/10.1016/j.nanoen.2017.04.036
Received 3 March 2017; Received in revised form 18 April 2017; Accepted 18 April 2017

alkyl chains are less concerned for organic electronics [28], particularly for PSCs. The factor that limits their talents is the larger steric hindrance effect (SHE), which could distort the π-conjugated backbone and result in wider bandgap (E_g) [29–31]. Very recently, we have reported that the cyclohexyl could distort the polymer backbone and help to improve the device V_{OC} in both the 4,7-bis(thiophen-2-yl) benzo[*c*] [1,2,5] thiadiazole (DTBT) and diketopyrrolopyrrole (DPP) based polymers [32,33]. However, the structure-property relationships of the ordered cyclic alkyl chains improving the device performances are still unknown, and the functions of cyclic alkyl chains that may impact the molecular arrangement and stacking are desired to be further deeply explored.

In this report, six benzo [1,2-*b*:4,5-*b′*]dithiophene (BDT) and DTBT alternated polymers (P–*R*) were synthesized with linear (pentyl, hexyl and heptyl) and cyclic (cyclopentyl, cyclohexyl and cycloheptyl) alkyl chains, the corresponding polymers were named as P–*n*5, P–*n*6, P–*n*7, P–*c*5, P–*c*6 and P–*c*7, respectively. The DTBT monomers show variable packing patterns depending on the types of alkyl chains, and meanwhile, the cyclic chains could also influence the physical and electrical properties of the polymers. Finally, for PSCs studies, employing 1,8-diiodooctane (DIO) as processing additive, the cyclic alkyl chains substituted polymers were found to give PCEs approaching 8% in PSCs blending with [6,6]-phenyl C_{71} butyric acid methyl-ester ($PC_{71}BM$), a significant improvement over their linear alkyl chains substituted counterparts, for which PCEs are lower than 6%. Our experiments indicated the cyclic alkyl chains promote the polymers rearranging into ordered micro-structures and forming interpenetrating networks with $PC_{71}BM$, which accelerate charge carrier transport. The substantial improvements of V_{OC}, J_{SC} and FF make cyclic alkyl chains promising candidates for designing high efficiency D–A type π-conjugated polymers.

2. Experimental section

2.1. General Information

Nuclear magnetic resonance (NMR) spectra were measured in $CDCl_3$ on a Bruker AVANCE 600 MHz Fourier transform NMR spectrometer; chemical shifts were quoted relative to the internal standard tetramethylsilane (TMS). High resolution mass spectra (HRMS) were obtained using a Bruker Maxis UHR–TOF, Ion Source: APCI system. The melting points of the monomers were measured using WRS–1B digital melting point apparatus, and confirmed by differential scanning calorimeter (PerkinElmer Diamond DSC, instrument DSC Q20 V24.11 Build 124) carried out under inert atmosphere with a scan speed of 10 °C/min. Absorption spectra were recorded with a Hitachi U–4100 UV–vis–NIR scanning spectrophotometer. The molecular weights of the polymers were measured by the gel permeation chromatography (GPC) performed using an ELEOS system, and polystyrene was used as the standard (room temperature, tetrahydrofuran (THF) as the eluent). The highest occupied molecular orbit (HOMO) energy levels, were determined by calculating the empirical formula of $E_{HOMO} = -e(E_{ox}+4.8-E_{1/2}{}^{(Fc/Fc+)})$ where E_{ox} was the onset oxidation potential. Bright field transmission electron microscopy (TEM) images were acquired using a HITACHI H–7650 electron microscope operating at an acceleration voltage of 100 kV. The film structures of the polymers and polymer/$PC_{71}BM$ blends were analyzed using X-ray diffraction (XRD, Bruker D8 ADVANCE). The grazing incidence X–ray diffraction (GIXD) data of the pure polymers and polymer/$PC_{71}BM$ blend films were obtained at beamline BL14B1 of the Shanghai Synchrotron Radiation Facility (SSRF) at a wavelength of 1.2398 Å and incident angle of 0.1 degree. BL14B1 is a beamline based on bending magnet and a Si (111) double crystal monochromator is employed to monochromatize the beam. The size of the focus spot is about 0.5 mm and the end station is equipped with a Huber 5021 diffractometer. NaI scintillation detector was used for data collection. GIXD patterns were recorded with a two-dimensional image detector. The single-crystals were obtained through slow evaporation of dichloromethane/hexane solution for DTBT–*c*6 (CCDC deposition no. 1497792), dichloromethane/methanol mixed solutions for DTBT–*c*5 (CCDC deposition no. 1497791) and DTBT–*c*7 (CCDC deposition no. 1497793). The X-ray crystal structures were performed on a Bruker Smart Apex II diffractometer (Mo *Ka* radiation, graphite monochromator, l =0.71073 Å, T=296 K). The structure was solved using SHELXS-97. CCDC deposition nos. 1497791, 1497792, 1497793 contains the supplementary crystallographic data for this paper.

2.2. PSC device fabrication and characterization

PSCs were fabricated as a standard device architecture, ITO/PEDOT:PSS/Polymer: $PC_{71}BM$/Ca/Al [34,35]. ITO coated glass substrates were ultrasonically cleaned sequentially in detergent, water, acetone and iso-propanol, followed by treating in an oxygen plasma (Plasma Preen II-862 Cleaner) for 6 min. The cleaned substrates were covered by a 40-nm-thick layer of PEDOT: PSS (Heraeus Clevios TM P AI 4083) by spin coating. After annealing in an oven at 150 °C for 20 min, the substrates were transferred to a glove box filled with N_2. Polymers and $PC_{71}BM$ (American Dye Source) were dissolved in *o*-DCB with or without DIO solvent. The solution was stirred overnight at room temperature, and then spin-coated on PEDOT:PSS modified ITO coated glass to form the active layer (~100 nm). The devices were completed after the deposition of Ca (10 nm)/Al (100 nm) as cathode through a shadow mask under high vacuum (~10^{-4} Pa). The thickness of the active layer was controlled by changing the spin speed during the spin-coating process and estimated using Veeco Dektak150 surface profiler. The effective area of the device was measured to be 0.1 cm^2. Current density–voltage (*J–V*) characteristics of the PSCs were recorded using Keithley 2420 source measurement unit under the illumination of AM 1.5 G (100 mW cm^{-2}, Newport solar simulator). Light intensity was calibrated with a standard silicon solar cell. The incident photon-to-electron conversion efficiency (IPCE) of solar cells were analyzed using a certified Newport IPCE measurement system.

Hole and electron mobility were measured using the space–charge–limited–current (SCLC) model [36], using device configuration of ITO/PEDOT:PSS/polymer: $PC_{71}BM$ (1:1.5)/Au or ITO/ZnO/polymer: $PC_{71}BM$ (1:1.5)/Ca/Al by taking current-voltage in the range of 0–5 V and fitting the results to a space charge limited form for hole-only or electron-only device. In the presence of carrier traps in the active layer, a trap–filled–limit (TFL) region exists between the ohmic and trap-free SCLC regions. The SCLC behavior in the trap-free region can be characterized by using the Mott-Gurney square law, where ε is the static dielectric constant of the medium and μ is the carrier mobility, V is the voltage drop across the device, and L is the thickness of active layer.

$$J = \frac{9\varepsilon\mu V^2}{8L^3}$$

3. Results and discussion

3.1. Physical properties

P–*R* were synthesized through Stille coupling polymerization of BDT and DTBT monomers according to the literature method [37], the polymer structures are shown in Fig. 1a, and the detailed synthetic routes of the monomers and polymers are shown in Scheme S1. The cyclic alkyl chains on the DTBT acceptors have little effect on the solubility of the polymers relative to linear alkyl chains, all the P–*R* are readily soluble in common organic solvents such as chloroform and 1,2-dichlorobenzene (*o*-DCB) at room temperature, enabling facile solution processing of PSC devices. P–*n*5, P–*n*7, P–*c*5 and P–*c*7 have relatively high number-average molecular weight (M_n >20 kg mol^{-1}),

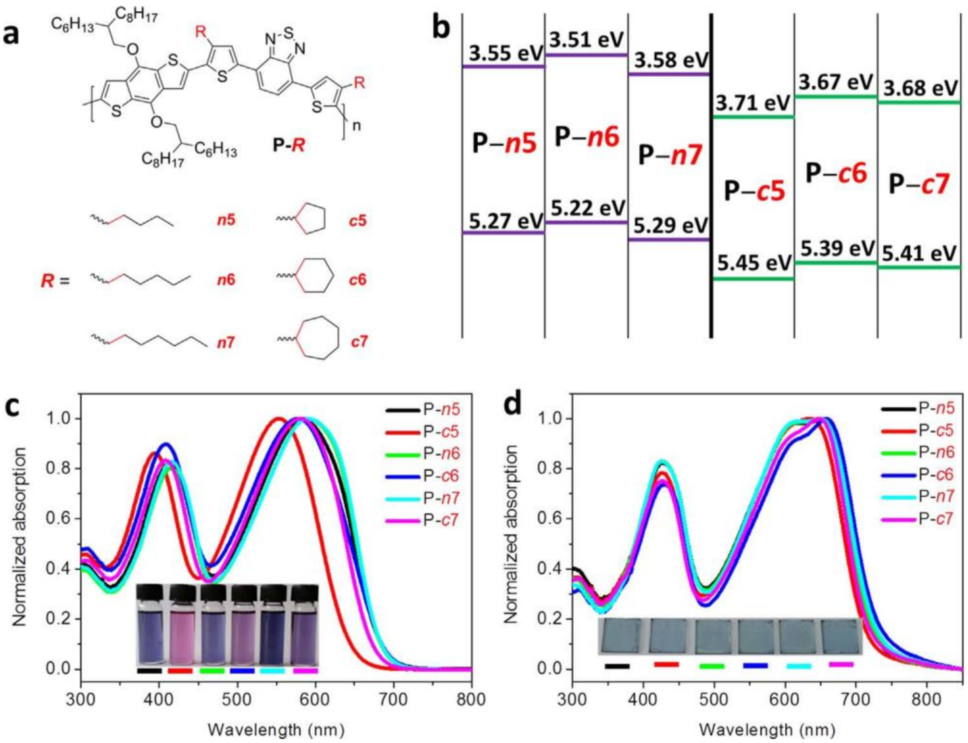

Fig. 1. (a) Chemical structure of P–*R*; (b) Energy level diagram for P–*R*; (c) UV–vis absorption spectra of P–*R* in *o*-DCB solutions at room temperature (inset: pictures of the solutions); (d) UV–vis absorption spectra of P–*R* in their pristine films (inset: pictures of the films).

comparable to that of previously reported P–*n*6 and P–*c*6 (Supporting Information). Cyclic voltammetry (CV) of the polymer films (Fig. S1) show that the cyclic alkyl chains substituted polymers possess higher ionization potential (*IP*) than linear chains, but meanwhile, the carbon numbers can slightly influence their *IP* values besides the types of the alkyl chains. Here, the steric cyclic alkyl chains twisting the polymer backbones increase the *IP*, as has been investigated through theoretical simulation and experimental studies [32]. The HOMO and the lowest unoccupied molecular orbital (LUMO) energy levels are described in Fig. 1b [38]. It has been previously shown that the alkyl chain can have a significant effect on the aggregation properties of the polymers, hence Fig. 1c compares the UV–vis absorption of polymers with linear and cyclic chains in dilute *o*-DCB solutions, P−*c*5, P−*c*6 and P−*c*7 exhibit relative hypochromatic absorption and distinct light colors as well, compared to P−*n*5, P−*n*6 and P−*n*7, respectively, indicating weaker aggregation characteristics. Their aggregates can be broken as the temperature elevating from 30–80 °C (Fig. S2). Polymers substituted with cyclic alkyl chains exhibit smaller peak shifts (Δλ) than that appended with *n*-alkyl analogs, especially for P−*c*5 (Δλ=5 nm), showing the weakest aggregation in solution. The temperature dependent UV–vis absorptions indicated that the inter-chain aggregates of P−*c*5, P−*c*6 and P−*c*7 have already been broken in a greater magnitude than that of P−*n*5, P−*n*6 and P−*n*7, respectively, when dissolving into *o*-DCB at room temperature from their agglomerative solid states. The distinctly different aggregation behaviors of the polymers depending on the type of side chains must be related to the arrangement of the cyclic and linear alkyl chains. However, as shown in Fig. 1d, the types of side chains will not influence their thin film absorption obviously, and all P–*R* show very similar absorption profiles and film colors with comparable E_g (1.71–1.74 eV). According to the recent studies, polymers having moderate aggregation are benefit for controlling of the morphology and phase separation in the polymer: fullerene blends [10].

Noting from Fig. 1d, for P−*c*6 and P−*c*7, distinct shoulder absorption centered at 658 and 647 nm, respectively, are observed, indicating potential ordered micro-structures in their films as has been proven in some other polymer systems [39,40]. The ordering of the P–*R* films fabricated by spin coating from *o*-DCB were investigated using XRD and two–dimensional GIXD (2D–GIXD). Seen from the XRD profiles (Fig. S3), no (010) diffraction (π-π stacking) is detected for all P–*R*, presumably that is attributed to the weaker crystalline nature of DTBT based polymers, many reports have confirmed the absence of (010) diffraction [41–43]. While for P−*c*6 and P−*c*7, obvious (100) diffraction (lamellar packing) peaks at 2θ=4.91° and 4.85°, respectively, are recorded, that implies well organized side chain packing patterns in these two polymers. In view of the similar polymer structure and same test conditions, the experimental results indicated cyclohexyl and cycloheptyl could promote the side chain interdigitation, and that result in higher degree of lamellar orders comparing with other side chain patterns. The lamellar packing in P−*c*6 and P−*c*7 are very compact with small *s* of ~ 1.80 nm and ~ 1.82 nm, respectively, which are smaller than some polymers appended with same 2–hexyldecyl chains [44,45]. The ordered lamellar packing and short spacing are beneficial for inter–chain interactions. Both P−*c*6 and P−*c*7 adopt preferential edge-on orientations as illustrated in their 2D-GIXD patterns (Fig. S4), which show partial arc at q_z (out-of-plane direction) values of 3.49 and 3.45 nm^{-1}, respectively, whereas, the other polymers do not show clear diffraction.

3.2. Crystal packing of DTBT based monomers

In order to definitely confirm the arrangement of the cyclic chains and better explain how the cyclic alkyl chains impact the molecular conformations and stacking, single-crystals of the DTBT based monomers DTBT−*c*5, DTBT−*c*6 and DTBT−*c*7 are prepared (Fig. 2 and Table S1, crystallographic data). We have also tried to cultivate the single crystals of DTBT−*n*5 and DTBT−*n*7, however, no crystals were obtained suitable for characterization, and hence only DTBT−*n*6 was used for comparison. Apparently, the cyclic alkyl chains could distort the monomer packing symmetry refer to naked DTBT [46], however, it is interesting to note that DTBT−cyclic chains have higher packing symmetries (monoclinic) than DTBT−*n*6 (triclinic) [41]. This finding reveals that the effect of cyclic alkyl chains which could destroy the

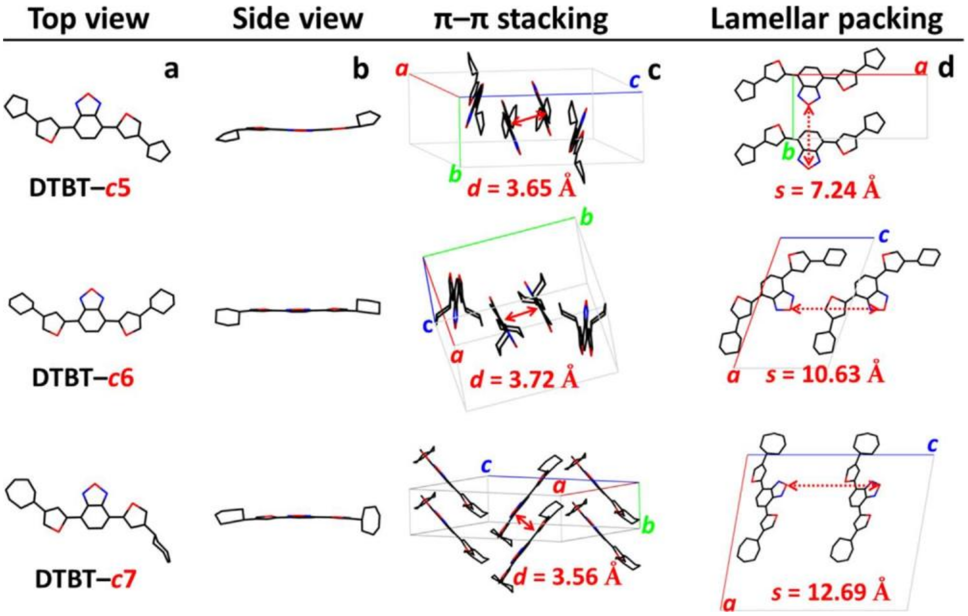

Fig. 2. (a) Crystal structures; (b) side view; (c) inter-planar π−π stacking; (d) lamellar packing. Atoms: carbon, black; nitrogen, blue; sulfur, red. Hydrogen atoms are omitted for clarity.

DTBT packing is weaker than linear chains such as hexyl. In addition, the DSC (Fig. S5) analysis of the monomers exhibited that the cyclic alkyl chains can significantly improve the melting points of the DTBTs compared to the linear chains substituted ones, which indicated stronger and tighter inter-molecular interactions in the case of DTBD−cyclic chains. As shown in Fig. 2a, DTBT−*c*5 and DTBT−*c*7 adopt *trans*– conformations, whereas DTBT−*c*6 has a fixed *cis*–conformation. Although there are reports inferring that the *cis*–DTBT may lead to more curved polymer backbone, and probably would affect the polymer inter-chain packing and charge carrier transporting [41,42], however, according to our studies, we found P–*c*6 has distinct advantages than P–*n*6 in their PSC devices [32]. We are more inclined to believe that the side chain ordering and arrangement rather than the molecular configuration will control their electrical properties of P–*R*. In spite of their different conformations, DTBT−*c*5, DTBT−*c*6 and DTBT−*c*7 are highly coplanar (Fig. 2b), that warrants effective π−π conjugation and charge transfer from electron–donating thiophene rings to central electron–withdrawing BT unit, which will determine the E_g of the final DTBT–based polymers [37].

The cyclopentyl, cyclohexyl and cycloheptyl are confirmed adopting *half-chair*, *chair* and *twist-chair* conformations in DTBT−*c*5, DTBT−*c*6 and DTBT−*c*7 crystals, respectively. As illustrated in Fig. 2c, the arrangements of the stereo chairs exhibit stronger inter-molecular steric hindrance than linear hexyl along the π−π stacking direction, resulting in π−π stacking distance (*d*) of ~3.65, ~3.72 and ~3.56 Å, respectively, being slightly larger than that in naked DTBT (~3.44–3.46 Å) [46] and DTBT−*n*6 (~3.38 Å) [41]. A large *d* value may not favor for inter-chain charge carrier transport, but in most cases, it could help to improve the open–circuit voltage (V_{OC}) [47–49]. As shown in Fig. 2d, the well-defined structures of cyclic chains can significantly promote the lamellar packing, which is quantified by calculating the sulfur–sulfur spacing of the adjacent BT units. This spacing is related to the number of the rings, the *s* of ~7.24 Å in DTBT−*c*5, ~10.63 Å in DTBT−*c*6 and ~12.69 Å in DTBT−*c*7 increases gradually with the increasing of the carbon numbers of the rings, interestingly, they are much smaller than that of DTBT−*n*6 (~1.509 nm) estimated from its crystal. The shorter *s* indicates the cyclic chains could decrease the steric hindrance in the lamellar packing directions, and benefit for more closer packing [50]. Although the monomer packing structures in the crystals could not directly explain the polymer aggregation characteristics, however, we infer the steric cyclic chains could hinder the π−π stacking in the polymers as well as in the monomers, and in turn, result in weak aggregation of the polymers. Meanwhile, the preferential conformations and arrangement of cyclic chains promote the micro-structure ordering of the polymers.

3.3. Photovoltaic performances

PSC devices with optimized P–*R*:$PC_{71}BM$ blend ratios (1:1.5 w/w) are fabricated from *o*-DCB with standard device architecture ITO/PEDOT:PSS/P–*R*:$PC_{71}BM$/Ca/Al throughout the study. Here, the device parameters of P−*n*6 and P−*c*6 are also included using our previous reported data. P−*c*5, P−*c*6 and P−*c*7 are less effective than P−*n*5, P−*n*6 and P−*n*7, respectively, in their polymer: $PC_{71}BM$ devices giving lower J_{SC} and FF (Fig. S6 and Table 1). In particular, P−*c*5 exhibited extremely low PCE ca. 1.29%, combining J_{SC} of 5.38 mA cm^{-2} and FF of 31.45%. However, surprisingly, when adding DIO to optimize the micro-structures in the active layers [7,51], the maximum PCEs of P−*c*5, P−*c*6 and P−*c*7 based devices improved impressively up to 7.72%, 7.86% and 7.90%, respectively. Nevertheless, P−*n*5, P−*n*6 and P−*n*7 based devices still show fair PCEs from 4.27% to 5.94%. The *J-V* and incident photon-to-electron conversion efficiency (IPCE) curves of the optimized PSC devices are shown in Fig. 3 and the device parameters are summarized in Table 1.

3.4. Polymer self-assembling properties

Here, using P−*c*5 and P−*n*5 as examples, the polymer self-assemblies in the active layers are investigated. Casting from *o*-DCB, the P−*c*5:$PC_{71}BM$ film exhibits light color (Fig. 4a, inset), being ascribed to its weak absorption between 500 and 700 nm (Fig. 4a), the absorption peak centered at 558 nm is very close to that of 554 nm in pure P−*c*5 absorption in solution (Fig. 1c), indicating P−*c*5 chains can hardly aggregate together as *o*-DCB drying. Therefore, the P−*c*5:$PC_{71}BM$ blend exhibits homogeneous phase determined from the transmission electron microscope (TEM, Fig. 4b) [52,53], which would obstruct the charge carrier inter-chain transporting and result in low hole mobility (μ_{hole}) of ~6.35×10^{-7} cm^2 V^{-1} s^{-1} (Fig. S7 and Table 1), all of which account for low J_{SC} and FF. Surprisingly, as 3% DIO is added, the reorganized blend exhibits stronger absorption in the charge transfer transition band of P−*c*5 as well as a deeper colored film (Fig. 4a).

Table 1
Summary of device parameters based on the active layers with polymer/$PC_{71}BM$ ratio (1:1.5) spun cast from *o*-DCB solutions with and without DIO.

Entry	DIO	V_{OC}	J_{SC}	FF	PCE (%)		μ_{hole}	μ_e
	(%)	(V)	(mA cm^{-2})	(%)	average[b]	max	($cm^2 V^{-1} s^{-1}$)	($cm^2 V^{-1} s^{-1}$)
P-n5	0	0.795	11.09	63.26	5.41	5.58	9.81×10^{-6}	5.91×10^{-4}
	1	0.756	11.21	50.22	4.08	4.27	1.64×10^{-5}	5.75×10^{-4}
P-c5	0	0.874	5.60	31.78	1.32	1.56	6.35×10^{-7}	6.65×10^{-4}
	3	0.820	13.76	69.20	7.59	7.72	1.87×10^{-4}	3.83×10^{-4}
P-n6[a]	0	0.80	11.13	69.78	6.09	6.21	3.08×10^{-5}	NA
	1	0.75	11.60	68.22	5.82	5.94	2.18×10^{-5}	NA
P-c6[a]	0	0.83	10.24	66.47	5.52	5.65	1.62×10^{-5}	NA
	3	0.80	13.50	72.74	7.72	7.86	3.46×10^{-5}	NA
P-n7	0	0.802	10.47	64.27	5.08	5.40	6.55×10^{-5}	6.07×10^{-4}
	1	0.754	10.72	60.41	4.76	4.88	2.52×10^{-5}	5.51×10^{-4}
P-c7	0	0.888	8.81	51.38	3.81	4.02	5.72×10^{-5}	8.64×10^{-4}
	4	0.815	13.85	70.00	7.73	7.90	6.54×10^{-4}	7.16×10^{-4}

[a] Data as reported in Ref. [29].
[b] The optimized 10 devices were considered for the estimation of device parameters.

Meanwhile, interpenetrating fibril-like micro-structures are observed from Fig. 4b, indicating P-*c*5 exhibits excellent self-assembly property, which help to improve the μ_{hole} significantly up to ~1.87×10^{-4} $cm^2 V^{-1} s^{-1}$, resulting in more balanced hole/electron mobility (μ_e is ~3.83×10^{-4} $cm^2 V^{-1} s^{-1}$). All the essential optical and electrical properties lead to increased incident photon-to-electron conversion efficiency (IPCE, Fig. 4c), and then better device performances with higher J_{SC} of 13.76 mA cm^{-2} and FF of 69.20%. Similar phenomena are found for P-*c*7 based devices (Table 1). However, as a striking contrast, the P-*n*5:$PC_{71}BM$ blend exhibits strong immunity on the effect of DIO, which shows almost identical absorption profiles, film colors and device IPCE curves (Fig. 4d and f). When DIO is added, the polymer micro-structures in P-*n*5: $PC_{71}BM$ and P-*n*7: $PC_{71}BM$ blends are less defined than in P-*c*5: $PC_{71}BM$ and P-*c*7: $PC_{71}BM$ (Fig. 4e and Fig. S8), respectively. These result in low μ_{hole} and unbalanced hole/electron transporting, which are correlated to the lower FFs comparing with P-*c*5 and P-*c*7 based devices. The simultaneously improved device parameters (V_{OC}, J_{SC} and FF) are highly desirable and it should be related to the structure dependent steric hindrance and arrangement of cyclic chains.

3.5. Micro-structure ordering of the polymer:$PC_{71}BM$ blends

The micro-structures of the polymers in their self-assembled blends are characterized using 2D–GIXD. As illustrated in Fig. 5a–c, P-*n*5, P-*n*6 and P-*n*7 show indistinct but discernible (100) diffractions at q_z=3.05, 2.89 and 2.82 nm^{-1}, corresponding to *s* of 2.06 nm, 2.18 nm and 2.23 nm, respectively. These partial arcs are characteristic of out-of-plane lamellar packing, indicating preferential edge-on orientations. In the patterns shown in Fig. 5d–f, P-*c*5, P-*c*6 and P-*c*7 exhibit rather pronounced (100) diffractions at q_z=3.29, 3.28 and 3.26 nm^{-1}, respectively, being consistent with preferential edge-on orientations relative to the substrate, and shorter *s* than that in P-*n*5, P-*n*6 and P-*n*7, respectively. In addition, P-*c*7 shows a discernible second-order diffraction in the out-of-plane direction, suggesting long-range order of the backbone [54]. The ordered structures of P-*c*5, P-*c*6 and P-*c*7 are well agreeing with the fibril-like structures in their TEM images. These observations confirm the advantages of cyclic chains in controlling the polymer self-assembly and promoting the lamellar packing order. Interestingly, we found from Fig. 5e that P-*c*6 shows a lamellar reflection in the in-plane direction with q_{xy}=3.30 nm^{-1} besides the out-of-plane diffraction at q_z=3.28 nm^{-1}, indicating the existence of face-on orientation for P-*c*6. That would promote the perpendicular charge carrier transport, and in turn, improve the performances of the BHJ solar cell [42,55]. The polymer micro-structures are also confirmed by out-of-plane XRD. As shown in Fig. S9, P-*c*5, P-*c*6 and P-*c*7 exhibit much stronger (100) diffractions and more closer packing than P-*n*5, P-*n*6 and P-*n*7, respectively.

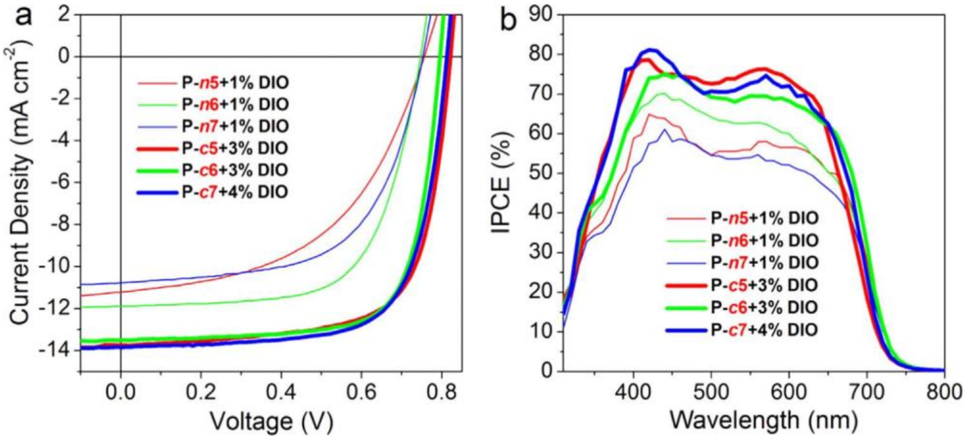

Fig. 3. *J-V* (a) and IPCE (b) curves of the optimized PSC devices. The polymer:$PC_{71}BM$ blend ratio is 1:1.5 w/w, and the DIO volume fraction is 1% for P-*n*5, P-*n*6 and P-*n*7, 3% for P-*c*5 and P-*c*6%, and 4% for P-*c*7.

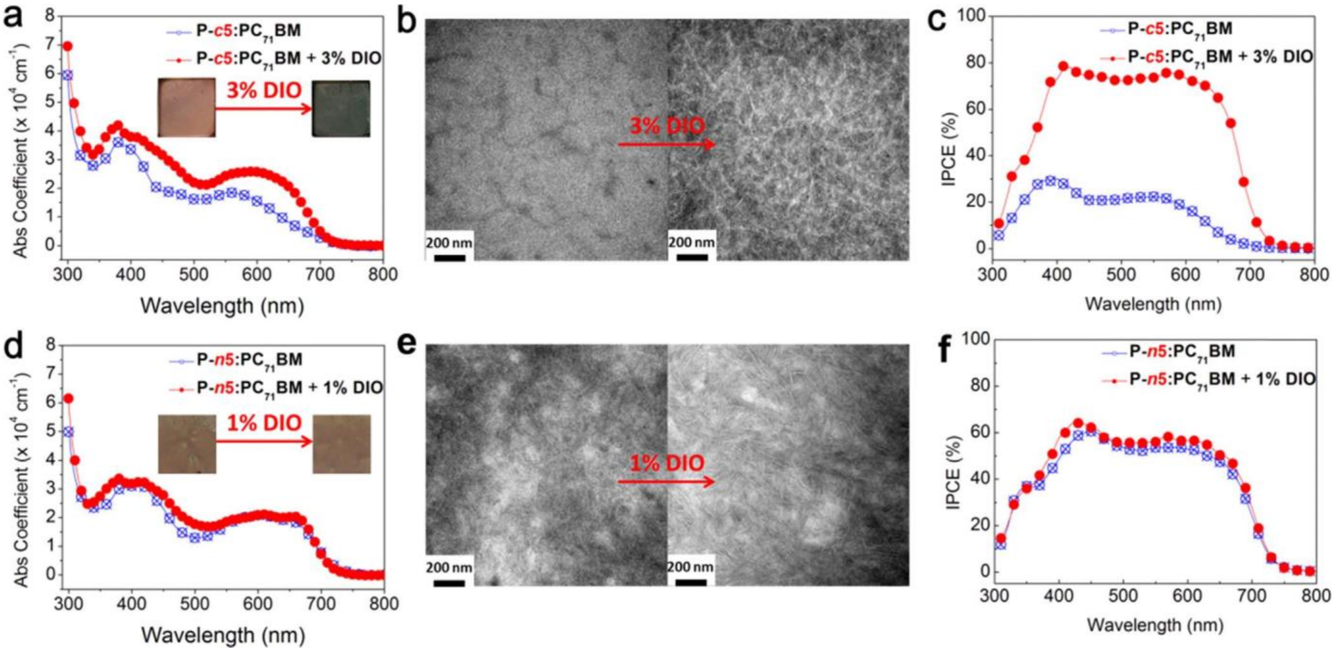

Fig. 4. (a) UV–vis absorption spectra of P−*c*5:$PC_{71}BM$ blends (inset: pictures of corresponding films); (b) TEM images of P−*c*5:$PC_{71}BM$ blends; (c) the IPCE curves P−*c*5:$PC_{71}BM$ blends; (d) UV–vis absorption spectra of P−*n*5:$PC_{71}BM$ blends (inset: pictures of corresponding films); (e) TEM images of P−*n*5:$PC_{71}BM$ blends; (f) the IPCE curves P−*n*5:$PC_{71}BM$ blends.

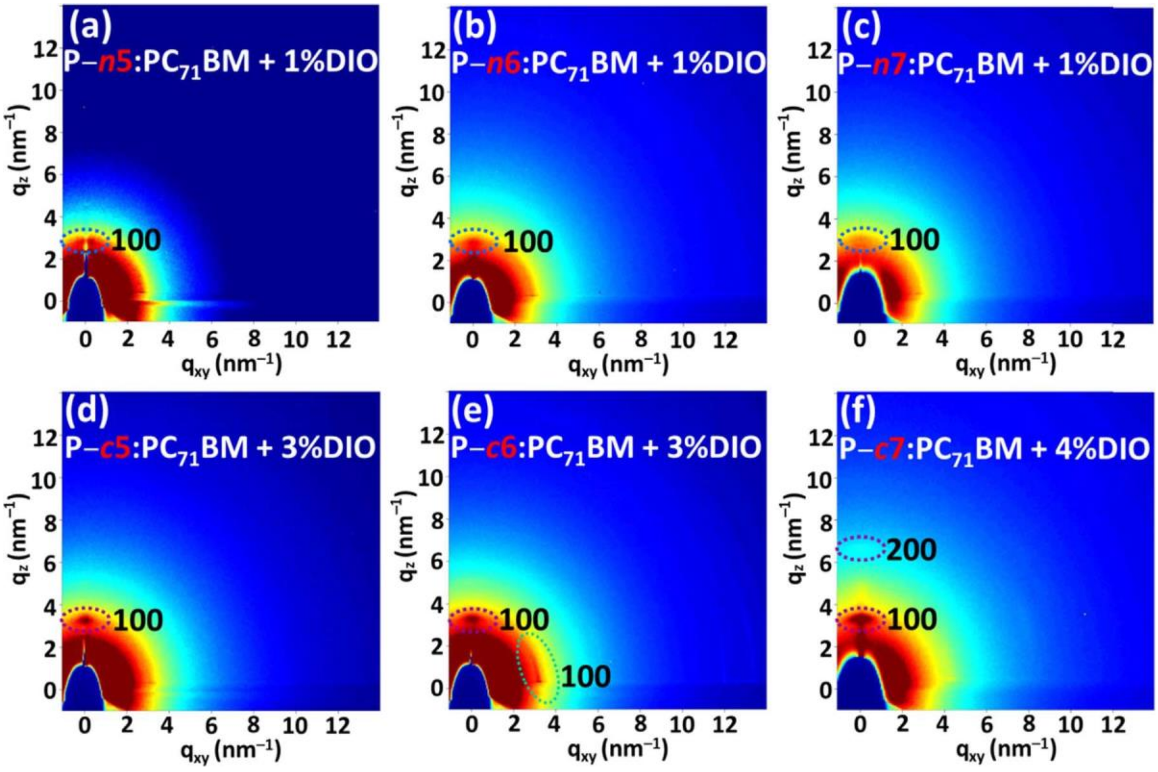

Fig. 5. 2D–GIXD patterns of P–*R*:$PC_{71}BM$ =1:1.5 cast from *o*-DCB + DIO solutions.

4. Conclusion

In summary, comparing the linear and cyclic alkyl chains on influencing the π–conjugated polymers' optical and electrical properties, we demonstrate firstly that the cyclic chains show distinct advantages on promoting the polymer self-assembling and packing properties. The cyclic chains have been proven to adopt preferential conformations in the crystals of the π–conjugated molecules, which could promote the crystal arranging symmetries and strengthen molecular packing patterns. The steric alkyl chains break the strong aggregation characteristics of the polymers, which make the controlling of the polymer self-assembling more effective, and in turn, improve the V_{OC} of the PSC devices. Using DIO as processing additive, P−*c*5, P−*c*6 and P−*c*7 reorganized into more ordered micro-structures with smaller side chain inter-chain lamellar spacing than P−*n*5, P−*n*6 and P−*n*7, respectively, in their polymer:$PC_{71}BM$ blends. The well-defined micro-structures enhanced the film absorption and balanced hole/electron transporting, which help to improve the J_{SC} and FF in the PSC devices. Finally, the PSC device performance improved significantly with substantial increased PCE. This study proposes that cyclic alkyl chains are promising candidates promoting the semi-conductor self-assembly and packing pattern for high performance solid state organic electronics.

Acknowledgements

This work was supported by the Ministry of Science and Technology of China (2014CB643501), the National Natural Science Foundation of China (51503219, 51573205 and 61405209), the Shandong Provincial Natural Science Foundation (ZR2015EQ002), the Qingdao Applied and Fundamental Research (16-5-1-94-jch), the Qingdao Institute of Bioenergy and Bioprocess Technology Director Innovation Foundation for Young Scientists (QIBEBT-DIFYS-201507).

Appendix A. Supplementary material

Supplementary data associated with this article can be found in the online version at doi:10.1016/j.nanoen.2017.04.036.

References

[1] G. Dennler, M.C. Scharber, C.J. Brabec, Adv. Mater. 21 (2009) 1323–1338.
[2] S.H. Park, A. Roy, S. Beaupre, S. Cho, N. Coates, J.S. Moon, D. Moses, M. Leclerc, K. Lee, A.J. Heeger, Nat. Photonics 3 (2009) 297–302.
[3] G. Yu, J. Gao, J.C. Hummelen, F. Wudl, A.J. Heeger, Science 270 (1995) 1789–1791.
[4] C. Winder, N.S. Sariciftci, J. Mater. Chem. 14 (2004) 1077–1086.
[5] W. Ma, C. Yang, X. Gong, K. Lee, A.J. Heeger, Adv. Funct. Mater. 15 (2005) 1617–1622.
[6] G. Li, V. Shrotriya, J. Huang, Y. Yao, T. Moriarty, K. Emery, Y. Yang, Nat. Mater. 4 (2005) 864–868.
[7] J.K. Lee, W.L. Ma, C.J. Brabec, J. Yuen, J.S. Moon, J.Y. Kim, K. Lee, G.C. Bazan, A.J. Heeger, J. Am. Chem. Soc. 130 (2008) 3619–3623.
[8] Y. Kim, S. Cook, S.M. Tuladhar, S.A. Choulis, J. Nelson, J.R. Durrant, D.D.C. Bradley, M. Giles, I. McCulloch, C.-S. Ha, M. Ree, Nat. Mater. 5 (2006) 197–203.
[9] P.M. Beaujuge, J.M.J. Fréchet, J. Am. Chem. Soc. 133 (2011) 20009–20029.
[10] Y. Liu, J. Zhao, Z. Li, C. Mu, W. Ma, H. Hu, K. Jiang, H. Lin, H. Ade, H. Yan, Nat. Commun. 5 (2014) 5293.
[11] J.-D. Chen, C. Cui, Y.-Q. Li, L. Zhou, Q.-D. Ou, C. Li, Y. Li, J.-X. Tang, Adv. Mater. 27 (2015) 1035–1041.
[12] Z. He, B. Xiao, F. Liu, H. Wu, Y. Yang, S. Xiao, C. Wang, T.P. Russell, Y. Cao, Nat. Photonics 9 (2015) 174–179.
[13] C.-C. Chen, W.-H. Chang, K. Yoshimura, K. Ohya, J. You, J. Gao, Z. Hong, Y. Yang, Adv. Mater. 26 (2014) 5670–5677.
[14] R.D. McCullough, S. Tristram-Nagle, S.P. Williams, R.D. Lowe, M. Jayaraman, J. Am. Chem. Soc. 115 (1993) 4910–4911.
[15] A. Babel, S.A. Jenekhe, Synth. Met. 148 (2005) 169–173.
[16] M. Gruber, S.-H. Jung, S. Schott, D. Venkateshvaran, A.J. Kronemeijer, J.W. Andreasen, C.R. McNeill, W.W.H. Wong, M. Shahid, M. Heeney, J.-K. Lee, H. Sirringhaus, Chem. Sci. 6 (2015) 6949–6960.
[17] A. Gadisa, W.D. Oosterbaan, K. Vandewal, J.-C. Bolsée, S. Bertho, J. D'Haen, L. Lutsen, D. Vanderzande, J.V. Manca, Adv. Funct. Mater. 19 (2009) 3300–3306.
[18] C.-H. Cho, H.J. Kim, H. Kang, T.J. Shin, B.J. Kim, J. Mater. Chem. 22 (2012) 14236–14245.
[19] C. Lee, H. Kang, W. Lee, T. Kim, K.-H. Kim, H.Y. Woo, C. Wang, B.J. Kim, Adv. Mater. 27 (2015) 2466–2471.
[20] J. Oh, K. Kranthiraja, C. Lee, K. Gunasekar, S. Kim, B. Ma, B.J. Kim, S.-H. Jin, Adv. Mater. 28 (2016) 10016–10023.
[21] J. Mei, Z. Bao, Chem. Mater. 26 (2014) 604–615.
[22] T. Lei, J.-Y. Wang, J. Pei, Chem. Mater. 26 (2014) 594–603.
[23] I. McCulloch, M. Heeney, C. Bailey, K. Genevicius, I. MacDonald, M. Shkunov, D. Sparrowe, S. Tierney, R. Wagner, W. Zhang, M.L. Chabinyc, R.J. Kline, M.D. McGehee, M.F. Toney, Nat. Mater. 5 (2006) 328–333.
[24] J.-H. Liao, M. Benz, E. Legoff, M.G. Kanatzidis, Adv. Mater. 6 (1994) 135–138.
[25] C. Kim, J. Liu, J. Lin, A.B. Tamayo, B. Walker, G. Wu, T.-Q. Nguyen, Chem. Mater. 24 (2012) 1699–1709.
[26] S. Saito, K. Nakakura, S. Yamaguchi, Angew. Chem. Int. Ed. 51 (2012) 714–717.
[27] L. Ding, H.-B. Li, T. Lei, H.-Z. Ying, R.-B. Wang, Y. Zhou, Z.-M. Su, J. Pei, Chem. Mater. 24 (2012) 1944–1949.
[28] A. Kraft, A.C. Grimsdale, A.B. Holmes, Angew. Chem. Int. Ed. 37 (1998) 402–428.
[29] M. Berggren, O. Inganas, G. Gustafsson, J. Rasmusson, M.R. Andersson, T. Hjertberg, O. Wennerstrom, Nature 372 (1994) 444–446.
[30] M. Berggren, G. Gustafsson, O. Inganäs, M.R. Andersson, O. Wennerström, T. Hjertberg, Adv. Mater. 6 (1994) 488–490.
[31] M.R. Andersson, M. Berggren, O. Inganaes, G. Gustafsson, J.C. Gustafsson-Carlberg, D. Selse, T. Hjertberg, O. Wennerstroem, Macromolecules 28 (1995) 7525–7529.
[32] L. Han, W. Chen, T. Hu, J. Ren, M. Qiu, Y. Zhou, D. Zhu, N. Wang, M. Sun, R. Yang, ACS Macro Lett. 4 (2015) 361–366.
[33] S. Wen, W. Chen, M. Fan, L. Duan, M. Qiu, M. Sun, L. Han, R. Yang, J. Mater. Chem. A 4 (2016) 18174–18180.
[34] L. Han, X. Bao, T. Hu, Z. Du, W. Chen, D. Zhu, Q. Liu, M. Sun, R. Yang, Macromol. Rapid Commun. 35 (2014) 1153–1157.
[35] Z. Ding, X. Long, B. Meng, K. Bai, C. Dou, J. Liu, L. Wang, Nano Energy 32 (2017) 216–224.
[36] G.G. Malliaras, J.R. Salem, P.J. Brock, C. Scott, Phys. Rev. B 58 (1998) R13411–R13414.
[37] H. Zhou, L. Yang, S. Xiao, S. Liu, W. You, Macromolecules 43 (2010) 811–820.
[38] J. Pommerehne, H. Vestweber, W. Guss, R.F. Mahrt, H. Bässler, M. Porsch, J. Daub, Adv. Mater. 7 (1995) 551–554.
[39] J. Kim, T.M. Swager, Nature 411 (2001) 1030–1034.
[40] X. Guo, N. Zhou, S.J. Lou, J.W. Hennek, R. Ponce Ortiz, M.R. Butler, P.-L.T. Boudreault, J. Strzalka, P.-O. Morin, M. Leclerc, J.T. López Navarrete, M.A. Ratner, L.X. Chen, R.P.H. Chang, A. Facchetti, T.J. Marks, J. Am. Chem. Soc. 134 (2012) 18427–18439.
[41] A.C. Stuart, J.R. Tumbleston, H. Zhou, W. Li, S. Liu, H. Ade, W. You, J. Am. Chem. Soc. 135 (2013) 1806–1815.
[42] I. Osaka, M. Shimawaki, H. Mori, I. Doi, E. Miyazaki, T. Koganezawa, K. Takimiya, J. Am. Chem. Soc. 134 (2012) 3498–3507.
[43] Y. Huang, F. Liu, X. Guo, W. Zhang, Y. Gu, J. Zhang, C.C. Han, T.P. Russell, J. Hou, Adv. Energy Mater. 3 (2013) 930–937.
[44] C.-Y. Mei, L. Liang, F.-G. Zhao, J.-T. Wang, L.-F. Yu, Y.-X. Li, W.-S. Li, Macromolecules 46 (2013) 7920–7931.
[45] N. Wang, Z. Chen, W. Wei, Z. Jiang, J. Am. Chem. Soc. 135 (2013) 17060–17068.
[46] C.B. Nielsen, A.J.P. White, I. McCulloch, J. Org. Chem. 80 (2015) 5045–5048.
[47] L. Yang, H. Zhou, W. You, J. Phys. Chem. C 114 (2010) 16793–16800.
[48] Y. Liang, D. Feng, Y. Wu, S.-T. Tsai, G. Li, C. Ray, L. Yu, J. Am. Chem. Soc. 131 (2009) 7792–7799.
[49] J.M. Szarko, J. Guo, Y. Liang, B. Lee, B.S. Rolczynski, J. Strzalka, T. Xu, S. Loser, T.J. Marks, L. Yu, L.X. Chen, Adv. Mater. 22 (2010) 5468–5472.
[50] D. Qian, W. Ma, Z. Li, X. Guo, S. Zhang, L. Ye, H. Ade, Za Tan, J. Hou, J. Am. Chem. Soc. 135 (2013) 8464–8467.
[51] J. Peet, J.Y. Kim, N.E. Coates, W.L. Ma, D. Moses, A.J. Heeger, G.C. Bazan, Nat. Mater. 6 (2007) 497–500.
[52] J.A. Love, C.M. Proctor, J. Liu, C.J. Takacs, A. Sharenko, T.S. van der Poll, A.J. Heeger, G.C. Bazan, T.-Q. Nguyen, Adv. Funct. Mater. 23 (2013) 5019–5026.
[53] Y. Huang, W. Wen, S. Mukherjee, H. Ade, E.J. Kramer, G.C. Bazan, Adv. Mater. 26 (2014) 4168–4172.
[54] T. Lei, J.-H. Dou, J. Pei, Adv. Mater. 24 (2012) 6457–6461.
[55] A. El Labban, J. Warnan, C. Cabanetos, O. Ratel, C. Tassone, M.F. Toney, P.M. Beaujuge, ACS Appl. Mater. Interfaces 6 (2014) 19477–19481.

Liangliang Han is an associate professor at Qingdao Institute of Bioenergy and Bioprocess Technology, Chinese Academy of Sciences. He received his Ph.D. degree from Changchun Institute of Optics, Fine Mechanics and Physics, Chinese Academy of Sciences in 2009 followed by working as a research associate at University of Hong Kong with Prof. Chi-Ming Che. His current research interests focus on design and synthesis of π–conjugated small molecules/polymers of organic electronics.

Huanxiang Jiang is a master student in University of Chinese Academy of Sciences (UCAS). He got his bachelor's degree in Qingdao University of Science and Technology. His major is material engineering. Currently, he is doing research in Qingdao Institute of Bioenergy and Bioprocess Technology, Chinese Academy of Sciences under the supervision of Prof. Renqiang Yang. His primary research interest is the device fabrication of polymer solar cells.

Dan Ouyang is a Ph.D. student in University of Hong Kong. She received her Master degree from Qingdao Institute of Bioenergy and Bioprocess Technology, Chinese Academy of Sciences under the supervision of Prof. Renqiang Yang in 2012, she works on conjugated polymers donor materials in organic solar cells. Her current research interests focus on hole-transporting materials.

Weichao Chen is an associate professor at Qingdao University. He received his Ph.D. degree from Changchun Institute of Applied Chemistry, Chinese Academy of Sciences in 2012 followed by working at Qingdao Institute of Bioenergy and Bioprocess Technology, Chinese Academy of Sciences. His current research interests focus on organic photovoltaic devices and thin film transistors.

Tong Hu received his master's degree from Ocean University of China, Material Physics and Chemistry, in 2015. During his graduate studies, He also worked as Prof. Renqiang Yang's visiting student at Qingdao Institute of Bioenergy and Bioprocess Technology, Chinese Academy of Sciences. His research focused on design and synthesis of π–conjugated polymers of organic electronics.

Junyi Wang is a postgraduate student at Qingdao Institute of Bioenergy and Bioprocess Technology, Chinese Academy of Sciences under the supervision of Prof. Renqiang Yang. He received his bachelor's degree from Ocean University of China in 2013. His major is the device optimization of organic photovoltaic devices.

Shuguang Wen is an associate professor at Qingdao Institute of Bioenergy and Bioprocess Technology, Chinese Academy of Sciences. He received his Ph.D. Degree from Lanzhou Institute of Chemical Physics, Chinese Academy of Sciences in 2008. His current research focus on design and synthesis of π–conjugated polymers, investigating the structure-property relationship for organic solar cells.

Mingliang Sun is a professor of materials science and engineering at the Ocean University of China. He received the B.S. degree from Qingdao University of Science and Technology, and the Ph.D. degree from Prof. Yong Cao's group in South China University of Technology. He was a visiting scholar in Prof. Qibing Pei's group from 2007 to 2008 in UCLA. He finished the Hong Kong scholar program from 2013 to 2014 in Prof. Chun-Sing Lee's group of City University of Hong Kong. He specializes in polymer synthesis for solar cells, light-emitting diodes, and light-emitting electrochemical cell applications.

Renqiang Yang is a professor at Qingdao Institute of Bioenergy and Bioprocess Technology (QIBEBT), Chinese Academy of Sciences. He received his Ph.D. degree from South China University of Technology in 2004 and then conducted his postdoctoral work at University of California Santa Barbara with Prof. Guillermo C. Bazan. In 2009, he joined QIBEBT. His research interests include molecular design and synthesis of advanced organic opto-electronic materials and thereof device applications.